High Surface Area Mesoporous Activated Carbon from Hemp Bast Fibre Using Hydrothermal Processing

Md Zakir Hossain, Wei Wu, William Z. Xu, Muhammad B.I. Chowdhury, Anil Kumar Jhawar, Devin Machin, Paul A Charpentier*

Department of Chemical and Biochemical Engineering, The University of Western Ontario, London, Ontario, Canada N6A 5B9

* Corresponding author

E-mail: pcharpentier@eng.uwo.ca

Western University

London, Ontario, Canada

N6A 5B9

Phone: 1 (519) 661-3466

Fax: 1 (519) 661-3498

Abstract

Synthesis of activated carbon from waste biomass is of current interest towards sustainability. The properties of biomass derived activated carbon largely depends on the carbonization process. This study reports preparing extremel high surface area mesoporous activated carbon from hemp bast fibre using hydrothermal processing. Processing in hot water (390-500ºC), then activation using KOH and NaOH was investigated at different loading ratios. The described approach was found to enhance the mesoporosity (centered at 3.0 to 4.5 nm) of the hemp derived activated carbon (HAC) from activation (confirmed by BJH pore size distribution and TEM imaging). BET results showed that the product has an extremely high surface area (2425 m^2/g) while the surface functional groups (-OH, COOH, C=C/C-C) were confirmed and quantified by XPS and FTIR results. Increasing KOH concentration was found to enhance the surface area with an optimum biochar to KOH ratio of 1:3. The crystallite domain size of HAC was determined using Raman spectroscopy of different wavelengths. The procedure described in this study is an environmentally friendly scalable route for the mass production of activated carbon using hemp fiber.

Keywords

Hemp bast fibre, hydrothermal processing, KOH activation, activated carbon.

Peer-reviewed version available at C 2018, 4, 38; doi:10.3390/c4030038

1. Introduction

Activated carbon is a wll-known porous material with large surface area and pore volume, being extensively used for gas separation, solvent recovery, contaminant removal from water, wastewater treatment and as a catalyst/catalyst support for different energy storage and conversion processes [1]. Recently, activated carbon is being extensively investigated for making carbon foams [2] and ultracapacitors/supercapacitors [3, 4], due to its porous structure. As the pore properties of activated carbon largely depend on the precursor materials and the synthesis method, different types of materials (natural and synthetic) have been examined as precursors. The most commonly used precursors for activated carbon production are coal, coconut shell, wood, agricultural wastes or industrial wastes [1]. Among them, biomass as a precursor is attracting significant attention as it is renewable, abundant, low cost, and eco-friendly.

Two basic activation processes, i.e., physical and chemical, are used to prepare activated carbonaceous materials from biomass [5]. Prior to either the physical or chemical activation process, the carbon precursor needs to be carbonized to produce char. If the formed char is activated using carbon dioxide or steam as the activating agent, the process is called physical activation [6]. If the char is activated in the presence of chemical agents, the process is termed chemical activation [7]. The step for char production can occasionally be skipped if chemical activation is employed. To obtain a well-developed pore structure in the final carbon product using physical activation, a significant amount of internal carbon mass removal is necessary. Activating agents used for chemical activation are dehydrating agents that enhance pyrolytic decomposition and prevent tar formation, thus enhancing the yield of carbon [5]. The most commonly used agents for chemical activation are acidic reagents such as $ZnCl_2$, H_3PO_4, HCl and H_2SO_4 or the basic reagents KOH, K_2CO_3, NaOH and Na_2CO_3. There is a growing interest in using alkali hydroxides as the activation agent, with KOH being one of the most promising

activating agents [8, 9]. In this work, KOH and NaOH are compared as activating agents while hemp bast fibre was chosen as the carbon precursor because of its unique fibrous structure to make carbonaceous materials [10]. Detailed structural and surface properties are very important for the application of the resultant product which was characterized in this work by various physio-chemical techniques including BET surface area and BJH pore size distribution, XRD, SEM, TEM, Raman, TGA, FTIR and XPS analysis.

2. Experimental

2.1 Materials

Hemp bast fibre was purchased from American Hemp, Winston Salem, NC, USA. KOH, NaOH and 36 to 40% HCl was obtained from Caledon Laboratories Ltd., Canada. Silica-alumina pellet was obtained from Micromeritics Instrument Corporation, Norcross, GA, USA. Powdered activated carbon (DARCO G-60, 100−325 mesh particle size) and Basolite® C300 were obtained from Sigma Aldrich Canada Co., Oakville, ON, Canada. Activated carbon, Norit Row 0.8mm pellets, steam activated were obtained from Alfa Aesar, Tewksbury, MA, USA. De-ionized (DI) water (18.2 MΩ) was taken from a compact ultrapure water system (EASY pure LF, Mandel Scientific Co., model BDI-D7381).

2.2 Preparation of HAC

Two hundred ml of DI water along with 12.0 g of pre-cut hemp bast fibre were sealed in a 600 ml Hastelloy C-276 reactor (Autoclave Engineers, Erie, Penn, U.S.A), and heated to the desired temperature (390, 450 or 500 ºC, respectively) and kept for 2 h. The resultant biochar was recovered by vacuum filtration and washed with DI water multiple times, then dried overnight at 120ºC in a vacuum oven. The dried biochar was thoroughly mixed with a desired amount of

KOH or NaOH using a mortar and pestle, then heated to 750 ºC (0.5ºC/min) and kept at 750°C for 1 h under Argon flow in a tubular furnace. The resulting product was thoroughly washed with dilute HCl followed by DI water until pH 7.0 was reached. Finally the products were dried overnight at 120 ºC in a vacuum oven. Activation of biochar using KOH to produce the final product was repeated at least three times.

2.3 Instrumentation

The Brunauer-Emmett-Teller (BET) surface area, pore diameter and pore volume of hemp derived activated carbon (HAC) and biochar were determined from nitrogen adsorption and desorption isotherm data obtained at −193 °C in a constant-volume adsorption apparatus (Tristar II 3020, Micromeritics Instrument Corporation) using 99.995% pure N_2 gas obtained from Praxair (Oakville, Canada). The prepared samples were degassed at 130 °C for 12 h to remove any moisture and other adsorbed gases from the surface. The pore size distributions were calculated using the BJH method from the desorption branch of the isotherms. The instrument calibration was examined by using the standard (silica-alumina pellets) obtained from the supplier (Micromeritics Instrument Corporation, Norcross, GA, USA). Calibration was also checked by using commercial activated carbons and Basolite where their specific surface areas are known. Details about the calibration results are provided in the supporting information.

X-ray diffraction (XRD) measurements were performed using a Bruker D2 PHASER desktop diffractometer using Cu Kα radiation (1.54 Å). The instrument was operated at 30 kV and 10 mA, using scan rate of 0.1° per second in the 2θ range from 10° to 70°. The morphology of the HAC was obtained using Scanning Electron Microscopy (Hitachi FlexSEM) (model SU 1000) with secondary electron detector and Transmission Electron Microscopy (TEM) (model JEOL 2010F). The X-ray photoelectron spectroscopy (XPS) analysis was carried out with a Kratos

Preprints (www.preprints.org) | NOT PEER-REVIEWED | Posted: 28 April 2018 doi:10.20944/preprints201804.0372.v1

Peer-reviewed version available at C 2018, 4, 38; doi:10.3390/c4030038

Axis Ultra spectrometer using a monochromatic AlK (alpha) source (15 mA, 14 kV). FTIR analysis of the hemp derived samples were examined using an ATR-FTIR spectroscope (Nicolet 6700 FTIR). Raman spectroscopy measurements were performed using a Kaiser Optical Systems RXNI-785 with an excitation wavelength of 785 nm. Crystallite domain size of the AC catalysts were measured using a Renishaw InVia Reflex Raman spectrometer with two additional wavelength lasers (633 nm and 514 nm). Thermogravimetric analysis (TGA) was conducted on a TA Q600 system with a heating rate of 10 ^{o}C/min from ambient temperature to 900 ^{o}C, in N_2 with a flow rate of 50 ml/min.

3. Results and discussion

Textural properties are critical for optimizing the application of any porous material. Textural properties of HAC prepared using hydrothermal processing are listed in Table 1, where the average values are reported after measuring three times. It is seen that the HAC obtained very high surface areas once activated by KOH or NaOH. KOH demonstrated advantages over NaOH in pore development of biochar. Both the BET and Langmuir surface areas slightly increase with increasing biochar synthesis temperature from 390 to 500 ^{o}C. Generally, the pore volume and pore size of the final product was found insensitive to the biochar synthesis temperature.

Table 1. Pore properties of HAC

Sample	Biochar synthesis temperature (^{o}C)	Activating reagent	Weight ratio of Biochar and activating reagent	BET surface area (m^2/g)	Langmuir surface area (m^2/g)	Pore volume (cm^3/g)	Average pore size (nm)
Hemp derived Biochar	--	--	--	2	3	0.001	--
HAC	390	KOH	1:1	1566	2078	0.810	4.6
	450	KOH	1:1	1587	2090	0.811	4.6
	500	KOH	1:1	1598	2101	0.813	4.6
	390	KOH	1:2	1992	2647	1.011	4.3
	390	KOH	1:3	2425	3363	1.216	2.9
	390	NaOH	1:1	1252	1673	0.662	4.3
	390	NaOH	1:2	1851	2525	0.925	3.1
	390	NaOH	1:3	2124	2848	1.017	2.9

Preprints (www.preprints.org) | NOT PEER-REVIEWED | Posted: 28 April 2018 doi:10.20944/preprints201804.0372.v1

Peer-reviewed version available at C 2018, 4, 38; doi:10.3390/c4030038

Table 2 compares the BET surface areas of activated carbon obtained in the present study with those using different feedstocks/activating reagent reported in the literature, with the present study showing the highest BET surface area of 2425 m^2/g. It is generally believed that the KOH activation process of any carbon material enhances the pore structure and morphology with a substantial increase in specific surface area [11].

Table 2. BET surface areas of activated carbons prepared from different sources of biomass as feedstocks

Biomass feedstocks	Activator used	BET surface area (m^2/g)
Walnut shell [12]	CO_2	379
Sunflower stem [12]	CO_2	438
Olive stone [12]	CO_2	438
Rice husk [13]	CO_2	446
Glucose/ovalbumin [14]	--	476
Pinewood [13]	CO_2	569
Glucose/borax [15]	--	614
Orange peel [16]	CO_2	618
Glucose [17]	KOH	1197
Palm date seed [18]	NaOH	1282
Desert shrub [19]	$ZnCl_2$	1296
Rice husk [20]	H_3PO_4	1498
Hazelnut shell [21]	KOH	1700
Glucose [22]	KOH	1704
Sucrose [23]	H_3PO_4	2120
Glucose [23]	NaOH	2129
Starch [24]	KOH	2190
Rye straw [25]	KOH	2200
Eucalyptus sawdust [26]	KOH	2252
Corncobs [27]	KOH	2300
Hemp bast fibre (this study)	KOH	2425

Figure 1 provides the N_2 adsorption-desorption isotherms at -193 ^oC and pore size distributions of HAC, where HAC was prepared using different biochar to KOH ratios at a synthesis temperature of 390^oC. All the adsorption-desorption isotherms exhibit a type IV isotherm with

a type IV hysteresis loop (according to IUPAC classification) in the relative pressure range from 0.4 to 1.0. Type IV isotherms are an indication for the existence of well-developed mesopores in the structure, whereas a type IV hysteresis loop indicates the formation of asymmetric, slit shaped mesopores, attributable to rapid gas evolution and open channels [28]. It has been observed that increasing the ratio of activating agent to biochar increases the textural properties (surface area and pore volume) significantly, attributed to increasing the etching effect of the activating reagent on the biochar surface, thus creating mesopores from micropores [29]. The unique mesoporous structure of hemp based HAC contributes to the high specific surface area and uniform pore size distribution. The activation temperature also plays an important factor for improving the specific surface area and pore volume. High temperature activation was previously shown to enhance porosity as previously confirmed by Wang et al. [30], while low temperatures were not favourable to increase porosity due to the low reaction rate between the activator and carbonaceous material. Wang et al. [30] obtained the highest BET surface area (2287 m^2/g) for making interconnected carbon nanosheets at 750 ^oC during the activation of biochar with KOH.

Preprints (www.preprints.org) | NOT PEER-REVIEWED | Posted: 28 April 2018 doi:10.20944/preprints201804.0372.v1

Peer-reviewed version available at C 2018, 4, 38; doi:10.3390/c4030038

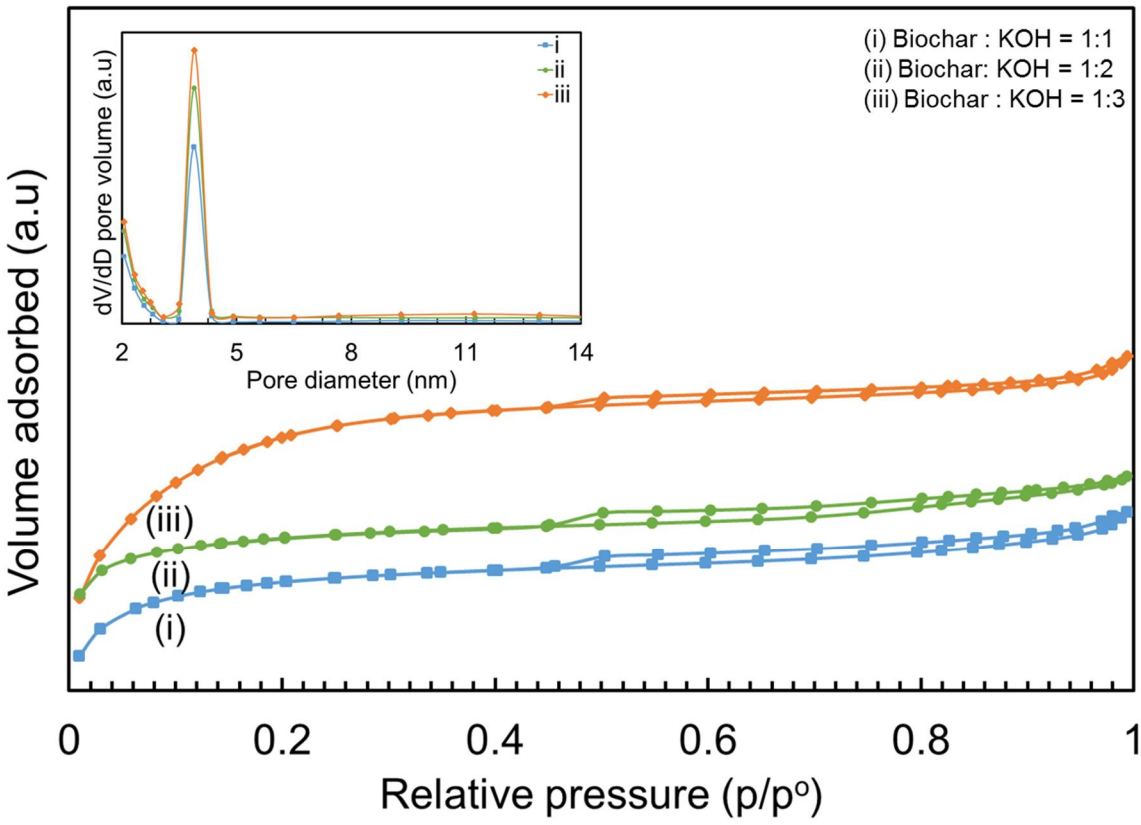

Figure 1. Nitrogen adsorption-desorption isotherms and BJH pore size distributions of HAC (inset).

Pore size distributions (PSD) of HAC prepared using different biochar to KOH ratios show that all the samples have a very narrow pore size distribution, mainly centred at 3.0 to 4.5 nm. This result is intriguing and indicates highly mesoporous carbon formation. Foo and Hameed [31] reported the average pore size of 21.44 nm of activated carbon produced from pistachio nut shells via microwave-induced chemical (KOH) activation. The same authors [32] also reported an average pore size of 34.14 and 26.89 nm for activated carbon from rice husk as a feedstock using KOH and K_2CO_3 activation. Tay et al. [7] synthesized different types of activated carbon from soybean oil cake and reported the average pore diameter of 5.23 nm of one of the product. Morphology of a material is a crucial factor for its application. The morphology of HAC was investigated and is presented in Figure 2 and Figure 3. Figure 2 shows the SEM images of the obtained hemp biochar (a) and HAC using different ratios of biochar to KOH at 1:1 (b), 1:2 (c)

and 1:3 (d). The observed HAC surface morphologies are very different than those from biochar. The biochar surface is rough with irregular sizes of particles and many large defect holes whereas the HAC surface shows the amorphous nature of carbon with a large mesopore content. The differences in morphologies among Figure 2(b), (c) and (d) suggest that KOH plays an important role for pore development of the resultant samples during activation. Figure 3(a) shows the TEM image of biochar whereas Figure 3(b), (c) and (d) shows the resulting HAC using different KOH ratios. Biochar does not have any pores whereas the activated carbon obtained using different biochar : KOH has a regular porous structure. This porous structure is advantageous for adsorption or catalysis, by providing more active sites. The TEM and SEM images corroborate the BET results. Lu et al. [33] found a similar mesoporous structure (adsorption average pore width = 3.23 nm) of activated carbon synthesized from corn straw.

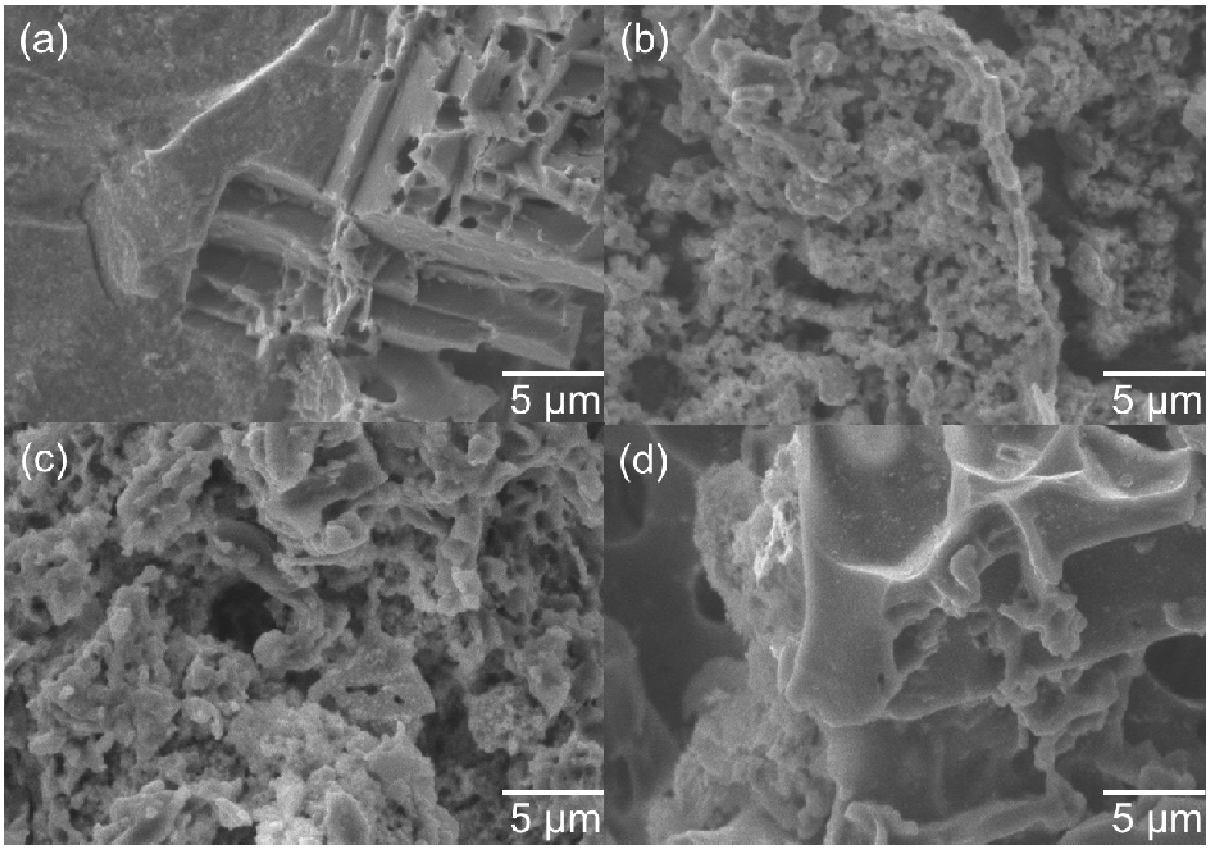

Figure 2. SEM images of (a) obtained biochar and HAC obtained using different ratios of biochar to KOH (b) 1:1 (c) 1:2 (d) 1:3.

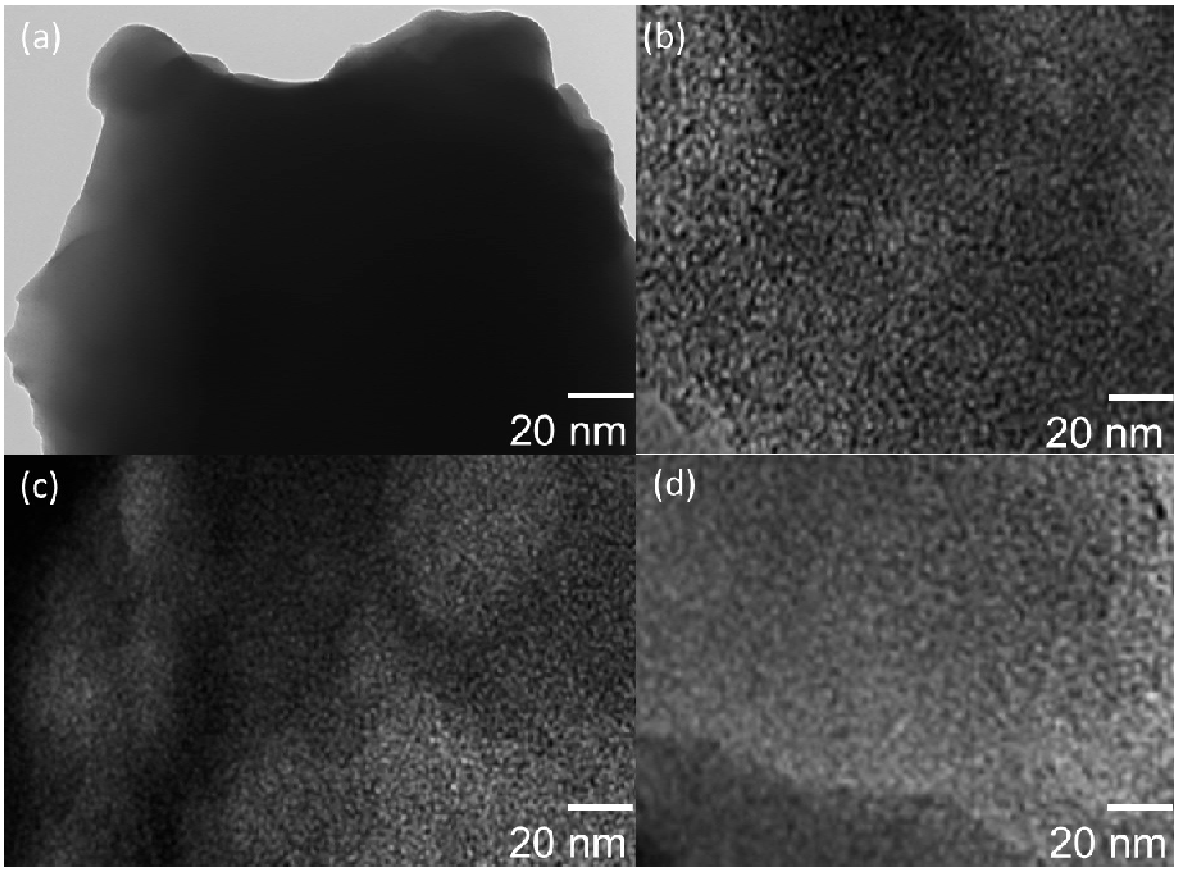

Figure 3. TEM images of (a) biochar and HAC obtained using different ratios of biochar to KOH (b) 1:1 (c) 1:2 (d) 1:3.

X-ray diffraction (XRD) was used to determine the crystalline structure of HAC. Figure 4 shows the small and large angle XRD patterns for the HAC samples. The small angle XRD pattern for all three samples indicates the formation of ordered hexagonal mesoporous structure [34]. This type of small angle XRD peak, is completely absent in commercial activated carbon, indicating the lack of long range porous structure [35]. The large peak at 23.4° 2θ [C(002) in Figure 4 corresponds to the amorphous carbon structure. The weak and broad C(100) peak at 2θ = 40-50° is attributed to the *a* axis of the graphite structure [36]. No significant differences were observed in the XRD patterns for all three investigated samples. This suggests that the different ratios of activating agent and biochar do not have a noticeable effect on the structural changes of HAC. Similar large angle XRD patterns were reported by Lu et al. [33] for the synthesis of mesoporous activated carbon from waste biomass material such as corn straw.

Preprints (www.preprints.org) | NOT PEER-REVIEWED | Posted: 28 April 2018 doi:10.20944/preprints201804.0372.v1

Peer-reviewed version available at C 2018, 4, 38; doi:10.3390/c4030038

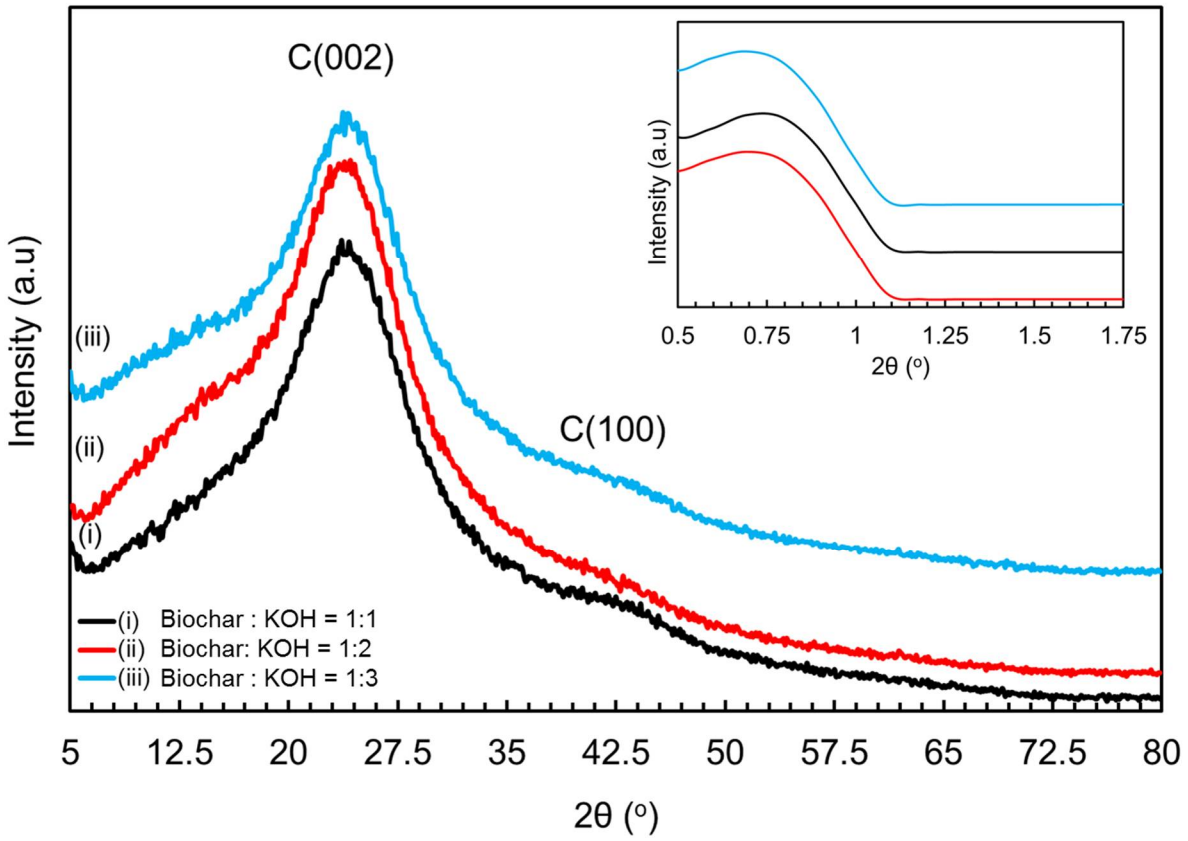

Figure 4. Large angle and small angle (inset) XRD patterns of the HAC.

The HAC samples were characterized by FTIR, with the spectra shown in Figure 5. The peak at 3288 cm^{-1} is attributed to O-H stretching while the peaks at 2977, 2941, 2914, and 2830 cm^{-1} are ascribed to asymmetric CH_3, asymmetric CH_2, symmetric CH_3, symmetric CH_2 stretching modes. The peak at 1447 cm^{-1} is attributable to CH_2 scissoring and CH_3 asymmetric bending modes. The peak at 1402 cm^{-1} can be assigned to O-H in-plane bending and CH_3 umbrella modes. The peak at 1109 cm^{-1} is attributable to CH_3 rocking or CH_2 wagging modes. The peak at 1016 cm^{-1} is mainly attributed to alcoholic C-O stretching mode. No significant difference is observed among the spectra of these samples, suggesting similar surface functional groups regardless of the biochar to KOH ratio. The presence of such functional groups was also reported by Barkauskas et al. [37] for commercial granulated activated carbon.

Preprints (www.preprints.org) | NOT PEER-REVIEWED | Posted: 28 April 2018 doi:10.20944/preprints201804.0372.v1

Peer-reviewed version available at C 2018, 4, 38; doi:10.3390/c4030038

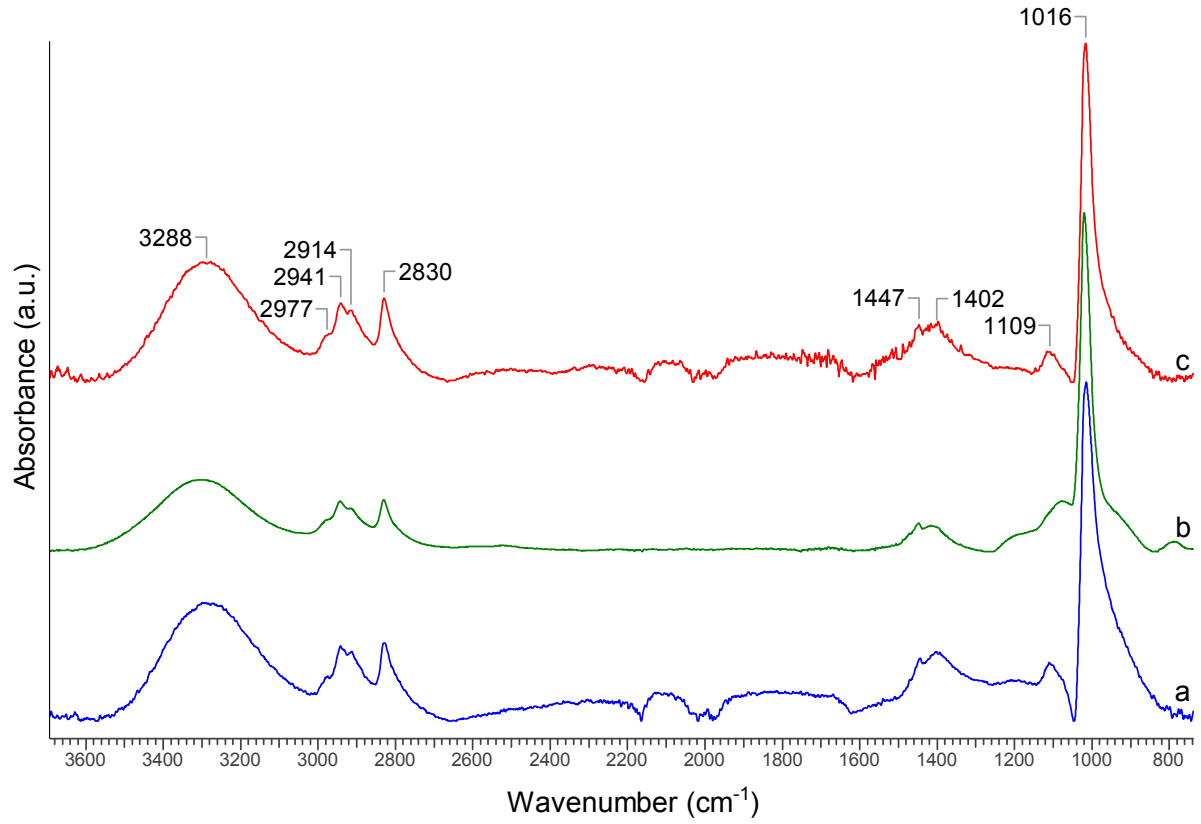

Figure 5. ATR-FTIR spectra of hemp derived activated carbon at different biochar and KOH ratio (a) 1:1 (b) 1:2 and (c) 1:3.

Raman spectroscopy was used to examine the ordered and disordered crystal structures of the hemp HAC. Figure 6 compares the Raman spectra of hemp derived activated carbon samples collected using a 785 nm laser. In these spectra, the G band at 1588 cm^{-1} corresponds to the first order scattering of E_{2g} mode and is related to the vibration of sp^2-bonded carbon atoms. The D band at 1315 cm^{-1} arises from a breathing mode of κ-point phonons of A_{1g} symmetry [38]. The D band corresponds to the amount of disorder and its intensity shows a degree of edge chirality [39]. By deconvoluting these peaks, the intensity ratios of D/G (I_D/I_G) were calculated and are listed in Table 3. The samples from the ratios of biochar to KOH at 1:1 and 1:2 demonstrated the same intensity ratio (I_D/I_G) of 1.37, which is lower than that (1.44) obtained from the ratio of biochar to KOH at 1:3. High I_D/I_G ratios suggest a high level of

Preprints (www.preprints.org) | NOT PEER-REVIEWED | Posted: 28 April 2018 doi:10.20944/preprints201804.0372.v1

Peer-reviewed version available at C 2018, 4, 38; doi:10.3390/c4030038

disorder such as defects, ripples and edges [40]. Besides, the full width at half maximum (FWHM) of G band (Γ_G) increased from 92.8 to 111.7 cm^{-1} when the ratio of biochar to KOH decreased from 1:1 to 1:3. As reviewed by Maslova et al. [41], higher Γ_G represents a larger amount of defects for carbonaceous materials.

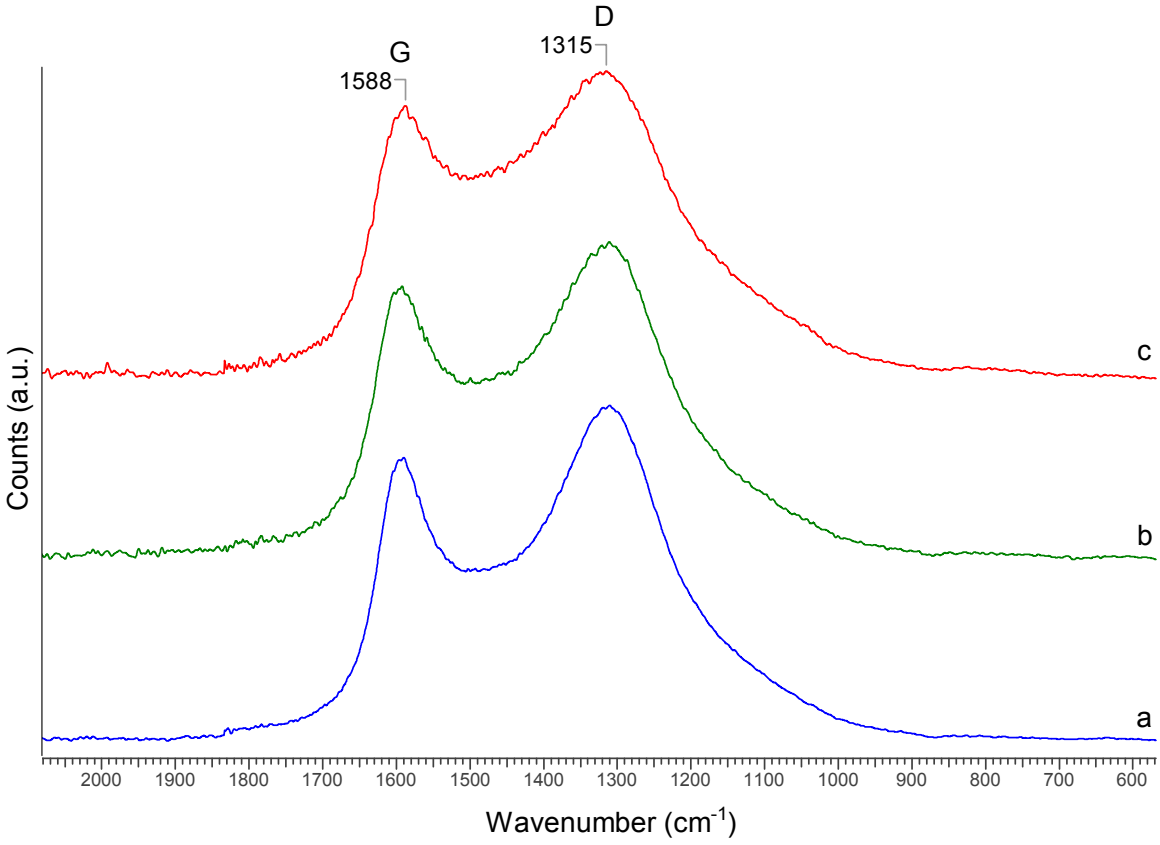

Figure 6. Raman spectra of hemp derived activated carbon at different biochar and KOH ratios (a) 1:1 (b) 1:2 and (c) 1:3.

It has been reported that the crystallite domain size (La) of carbonaceous materials can be calculated using the equation $La=C(\lambda_L)/(I_D/I_G)$ where a linear relationship $C(\lambda_L) \approx C_0 + \lambda_L C_1$ is valid in the excitation wavelength range of 400 nm < λ_L < 700 nm where C_0 = -12.6 nm and C_1=0.033 [42]. In order to study the domain size of the hemp HAC samples, the Raman spectra of these samples were also collected using two other laser sources with wavelengths of 633 nm and 514 nm, respectively. The I_D/I_G and La values were calculated and are listed in Table 3. According to these results, the domain sizes of the samples obtained from biochar to KOH

ratios of 1:1 and 1:2 are similar, but larger than those obtained using a biochar to KOH ratio of 1:3. These results are in good agreement with the Raman results measured using the 785 nm laser, i.e., the crystallite domain size did not change much when the ratio of biochar to KOH changed from 1:1 to 1:2, but decreased when the ratio of biochar to KOH changed to 1:3.

Table 3. Raman results of the HAC samples obtained from different biochar to KOH ratios.

Ratios	λ=785 nm		λ=633 nm		λ=514 nm	
	I_D/I_G	Γ_G (cm^{-1})	I_D/I_G	La (nm)	I_D/I_G	La (nm)
1:1	1.37	92.8	1.112±0.007	7.46±0.05	1.008±0.043	4.33±0.18
1:2	1.37	102.2	1.105±0.035	7.50±0.24	1.028±0.017	4.24±0.07
1:3	1.44	111.7	1.191±0.016	6.96±0.09	1.071±0.020	4.07±0.08

The surface chemistry of HAC was characterized using X-ray photoelectron spectroscopy (XPS). XPS survey spectra of HAC's is summarized in Figure 7(a) and Table 4. Figure 7a and Table 4 show that increasing the biochar to KOH ratio increases the atomic percentages of O (from 16.6 to 24.2%) and decreases the atomic percentages of C (80 to 70.7%). Similar trends were confirmed by Tai et al. [43] for synthesizing activated carbon from graphite using different KOH ratios. The atomic percentage of Si also slightly increased (from 2.3 to 4.2%) with increasing ratios. Si is the second most abundant element in soils which is found in substantial amount in many plants [44]. Higher amounts of KOH helped to precipitate higher Si on the surface of HAC.

Preprints (www.preprints.org) | NOT PEER-REVIEWED | Posted: 28 April 2018 doi:10.20944/preprints201804.0372.v1

Peer-reviewed version available at C 2018, 4, 38; doi:10.3390/c4030038

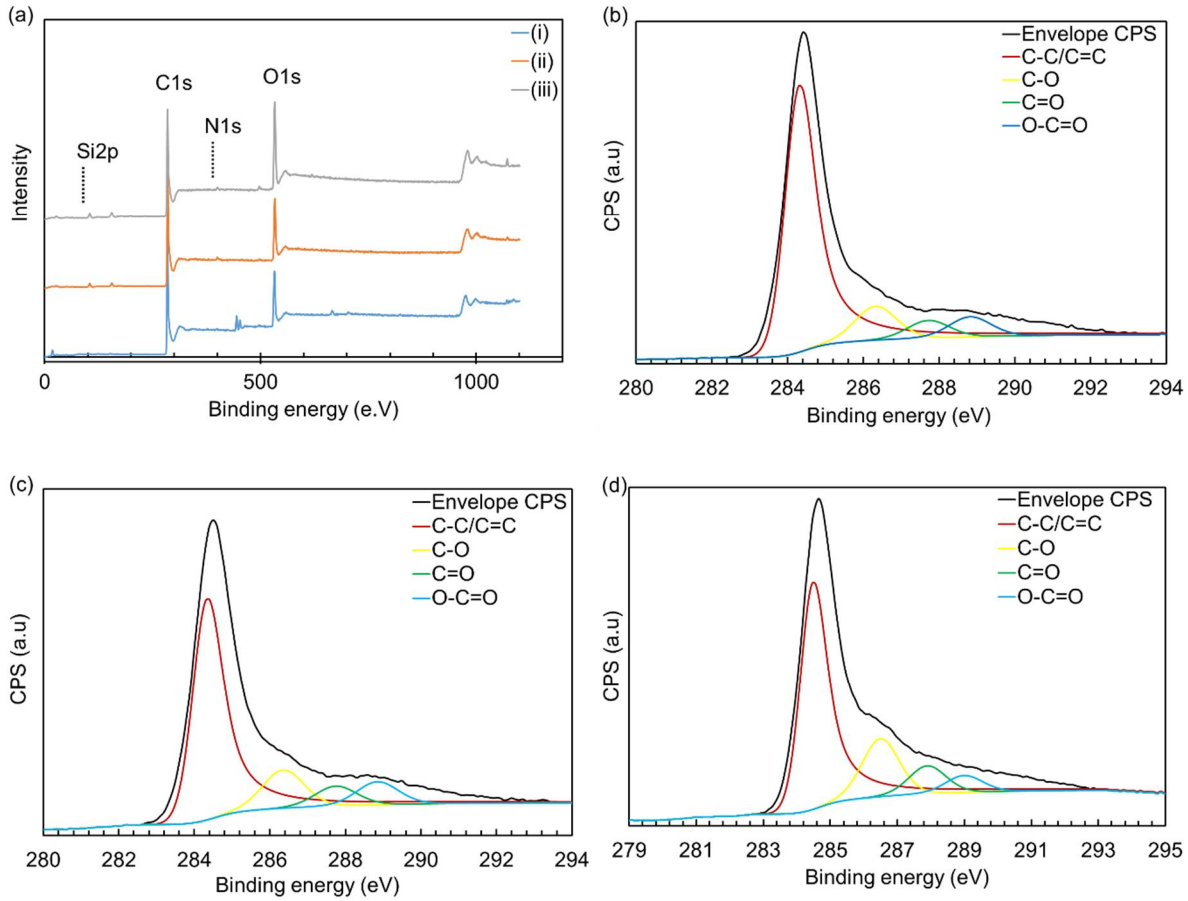

Figure 7. (a) XPS Survey spectra of HAC obtained using different ratios of biochar to KOH (i) 1:1 (ii) 1:2 (iii) 1:3; High resolution C(1s) XPS spectra of resultant HAC obtained using different ratios of biochar to KOH (a) 1:1 (b) 1:2 (c) 1:3.

Table 4. Atomic percentages of the elements present in the surfaces of carbonaceous materials with different biochar to KOH ratios.

Ratios	Atomic percentages			
	C	O	N	Si
1:1	80.0	16.6	1.1	2.3
1:2	73.1	22.4	1.1	3.4
1:3	70.7	24.2	0.9	4.2

Table 5. Relative contents of carbon species present in the carbonaceous materials based on XPS survey spectra.

Ratios	Percentages of relative content			
	C-C/C=C	C-O	C=O	O-C=O
1:1	78.3	10.3	5.4	6.0
1:2	76.1	11.2	5.9	6.8
1:3	75.1	12.2	6.5	6.2

The C(1s) XPS spectra of the resultant HAC is shown in Figure 7(b), (c) and (d) with the four most prominent deconvoluted components of the C(1s) envelope shown in each panel. Relative contents of carbon species present in HAC's based on the XPS survey spectra are presented in Table 5 The binding energy of 284.5 eV is attributed to the C–C, C=C and C–H bonds. Moreover, the binding energies of 286.4, 287.8 and 289.1 eV are typically assigned to the C–OH, C=O, and O=C–OH functional groups, respectively [45]. Deconvolution of all the C(1s) spectra resulted in a main peak located at 284.4 eV, corresponding to the C–C, C=C and C–H bonds. In Figure 7(b), (c) and (d), deconvolution of the C(1s) peak of the HAC resulted in three peaks located at binding energies of 286.4, 287.8 and 289.1 eV, which are attributed to the C–OH, C=O and O=C–OH functional groups, respectively. Usually, the C(1s) XPS spectrum of commercial activated carbon shows four similar components that correspond to carbon atoms in different functional groups: the non-oxygenated C at 284.5 eV for C=C/C-C in aromatic rings, the C in C–O bonds at 286.4 eV for epoxy and alkoxy, the carbonyl C at 287.8 eV for C=O, and the carboxylate carbon at 289.1 eV for O–C=O [46]. Relative percentages of oxygenated functional groups increase with increasing biochar to KOH ratios, whereas the non-oxygenated functional group slightly decreases (Table 5).

TG-DTA of HAC under nitrogen atmosphere was investigated for thermal stability, which is shown in Figure 8. No significant mass loss was detected when the material was heated up to 1000ºC, except a slight mass loss below 100ºC which was attributed to the loss of water.

Preprints (www.preprints.org) | NOT PEER-REVIEWED | Posted: 28 April 2018 doi:10.20944/preprints201804.0372.v1

Peer-reviewed version available at C 2018, 4, 38; doi:10.3390/c4030038

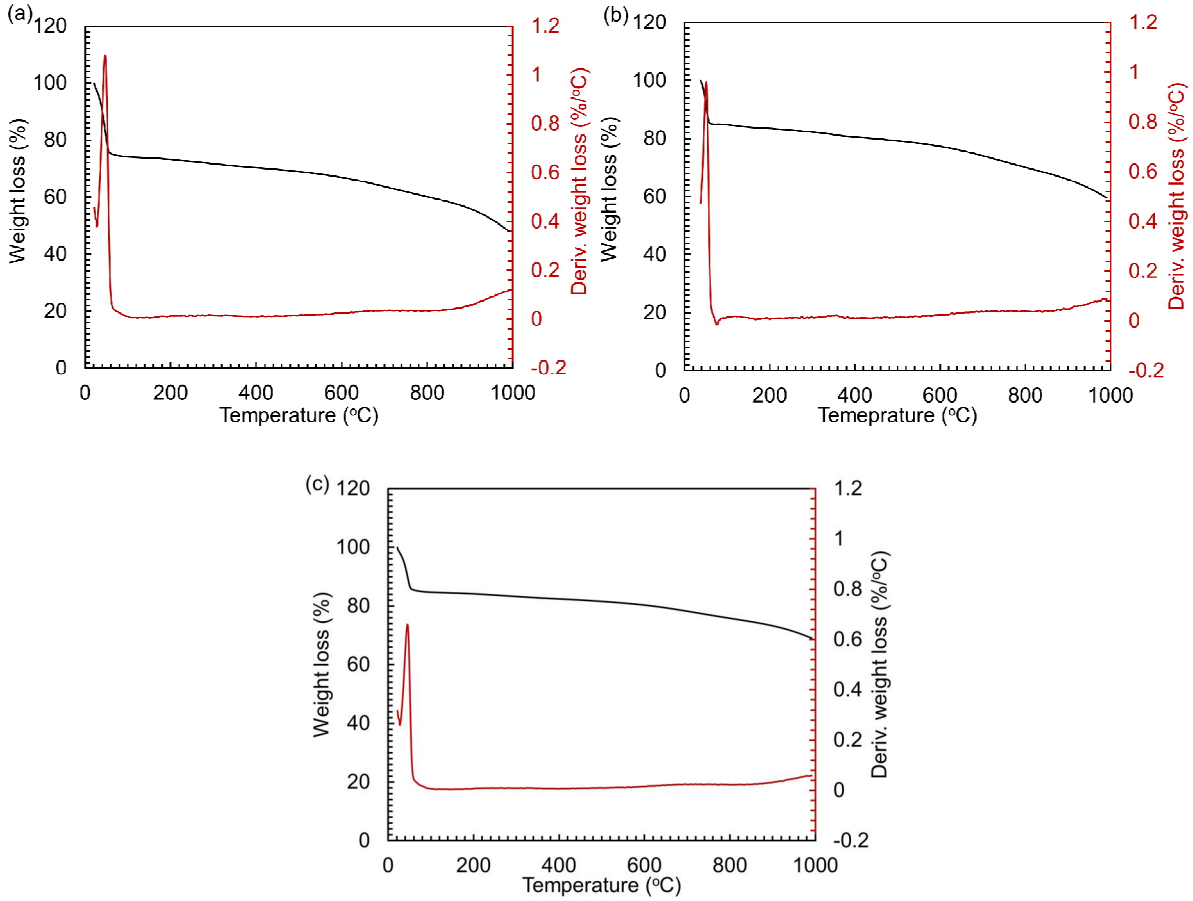

Figure 8. TG-DTA curves for hemp derived activated carbon obtained using different ratios of biochar to KOH (a) 1:1 (b) 1:2 and (c) 1:3.

As shown above, both KOH and NaOH provide high surface area activated carbon from hemp fiber biochar. Either KOH or NaOH are believed to act as dehydrating agents which influence the pyrolytic decomposition and inhibit the formation of tar, thus enhancing the yield of carbon. Impregnation of KOH into the biochar first results in degradation of the cellulosic material and then carbonization, leading to dehydration that results in charring and aromatization of the carbon skeleton and creation of the porous structure [47]. Pore structure with resultant high surface area is formed by rigorous evolution of gaseous by-products during KOH activation. According to the chemical activation mechanism [48, 49], it is suggested that during activation, the chemical reaction between KOH and carbon proceeds as $6KOH + 2C = 2K + 3H_2 + 2K_2CO_3$, followed by either decomposition of K_2CO_3 or reaction of $K/K_2CO_3/CO_2$ with carbon, the production of H_2 will potentially open up the pores. More importantly, according to Viculis

et al. [50], potassium might play an important role in greatly increasing the surface area. The produced potassium atoms form an intercalation compound, KC_8. Upon treatment with water after activation, the reaction between potassium intercalated compounds and aqueous solvent opens up the pores [50]. As shown in Table 1, it was found that with increased KOH loading in the activation reaction, the surface area of the resulting product increased, being consistent with this mechanism.

4. Conclusion

- Hemp fiber derived highly mesoporous activated carbon (HAC) with large surface area and pore volume was synthesized.
- Synthesis temperature of intermediate product (biochar) was found insensitive to final product.
- Surface morphologies of HAC was confirmed using several physico-chemical techniques such as BET, SEM, TEM, XRD, FTIR, Raman and XPS analysis.

Acknowledgements

This work is supported by Natural Sciences & Engineering Research Councils (NSERC) of Canada & BioFuelNet Canada.

References

[1] A. Jain, R. Balasubramanian, M. Srinivasan, Hydrothermal conversion of biomass waste to activated carbon with high porosity: A review, Chemical Engineering Journal 283 (2016) 789-805.

[2] X. Li, S. Liu, Y. Huang, Y. Zheng, D.P. Harper, Z. Zheng, Preparation and Foaming Mechanism of Pyrocarbon Foams Controlled by Activated Carbon as the Transplantation Core, ACS Sustainable Chemistry & Engineering (2018).

[3] M.-H. Kim, K.-B. Kim, S.-M. Park, K.C. Roh, Hierarchically structured activated carbon for ultracapacitors, Scientific reports 6 (2016) 21182.
[4] H. Ba, W. Wang, S. Pronkin, T. Romero, W. Baaziz, L. Nguyen-Dinh, W. Chu, O. Ersen, C. Pham-Huu, Biosourced Foam-Like Activated Carbon Materials as High-Performance Supercapacitors, Advanced Sustainable Systems (2018).
[5] R. Bansal, J. Donnet, STOECKLI,"Active Carbon", Marcell Dekker, New York and Bansel, 1988.
[6] R. Bardestani, S. Kaliaguine, Steam activation and mild air oxidation of vacuum pyrolysis biochar, Biomass and Bioenergy 108 (2018) 101-112.
[7] T. Tay, S. Ucar, S. Karagöz, Preparation and characterization of activated carbon from waste biomass, J. Hazard. Mater. 165(1-3) (2009) 481-485.
[8] S. Li, K. Han, J. Li, M. Li, C. Lu, Preparation and characterization of super activated carbon produced from gulfweed by KOH activation, Microporous and Mesoporous Materials 243 (2017) 291-300.
[9] M. Afdhol, R. Amiliana, A. Hanafi, Preparation of Activated Carbon from Palm Shells Using KOH and ZnCl2 as the Activating Agent, IOP Conference Series: Earth and Environmental Science, IOP Publishing, 2017, p. 012009.
[10] R. Sui, A.S. Rizkalla, P.A. Charpentier, Synthesis and Formation of Silica Aerogel Particles By a Novel Sol- Gel Route in Supercritical Carbon Dioxide, J. Phys. Chem. B 108(32) (2004) 11886-11892.
[11] V. Subramanian, C. Luo, A. Stephan, K. Nahm, S. Thomas, B. Wei, Supercapacitors from activated carbon derived from banana fibers, The Journal of Physical Chemistry C 111(20) (2007) 7527-7531.
[12] S. Roman, J.V. Nabais, B. Ledesma, J. González, C. Laginhas, M. Titirici, Production of low-cost adsorbents with tunable surface chemistry by conjunction of hydrothermal carbonization and activation processes, Microporous and Mesoporous Materials 165 (2013) 127-133.
[13] Z. Liu, F.-S. Zhang, Removal of copper (II) and phenol from aqueous solution using porous carbons derived from hydrothermal chars, Desalination 267(1) (2011) 101-106.
[14] R.J. White, N. Yoshizawa, M. Antonietti, M.-M. Titirici, A sustainable synthesis of nitrogen-doped carbon aerogels, Green chemistry 13(9) (2011) 2428-2434.
[15] T.P. Fellinger, R.J. White, M.M. Titirici, M. Antonietti, Borax-Mediated Formation of Carbon Aerogels from Glucose, Advanced Functional Materials 22(15) (2012) 3254-3260.
[16] M. Fernandez, B. Ledesma, S. Román, P. Bonelli, A. Cukierman, Development and characterization of activated hydrochars from orange peels as potential adsorbents for emerging organic contaminants, Bioresource technology 183 (2015) 221-228.
[17] F. Gao, G. Shao, J. Qu, S. Lv, Y. Li, M. Wu, Tailoring of porous and nitrogen-rich carbons derived from hydrochar for high-performance supercapacitor electrodes, Electrochimica Acta 155 (2015) 201-208.
[18] M.A. Islam, I. Tan, A. Benhouria, M. Asif, B. Hameed, Mesoporous and adsorptive properties of palm date seed activated carbon prepared via sequential hydrothermal carbonization and sodium hydroxide activation, Chemical Engineering Journal 270 (2015) 187-195.
[19] X. Zhu, Y. Liu, F. Qian, C. Zhou, S. Zhang, J. Chen, Role of hydrochar properties on the porosity of hydrochar-based porous carbon for their sustainable application, ACS Sustainable Chemistry & Engineering 3(5) (2015) 833-840.
[20] L. Ding, B. Zou, Y. Li, H. Liu, Z. Wang, C. Zhao, Y. Su, Y. Guo, The production of hydrochar-based hierarchical porous carbons for use as electrochemical supercapacitor electrode materials, Colloids and Surfaces A: Physicochemical and Engineering Aspects 423 (2013) 104-111.

[21] E. Unur, S. Brutti, S. Panero, B. Scrosati, Nanoporous carbons from hydrothermally treated biomass as anode materials for lithium ion batteries, Microporous and Mesoporous Materials 174 (2013) 25-33.
[22] Y. Gong, H. Wang, Z. Wei, L. Xie, Y. Wang, An efficient way to introduce hierarchical structure into biomass-based hydrothermal carbonaceous materials, ACS Sustainable Chemistry & Engineering 2(10) (2014) 2435-2441.
[23] A.J. Romero-Anaya, M. Ouzzine, M. Lillo-Ródenas, A. Linares-Solano, Spherical carbons: synthesis, characterization and activation processes, Carbon 68 (2014) 296-307.
[24] M. Sevilla, A.B. Fuertes, Sustainable porous carbons with a superior performance for CO 2 capture, Energy & Environmental Science 4(5) (2011) 1765-1771.
[25] C. Falco, J.P. Marco-Lozar, D. Salinas-Torres, E. Morallon, D. Cazorla-Amorós, M.-M. Titirici, D. Lozano-Castelló, Tailoring the porosity of chemically activated hydrothermal carbons: influence of the precursor and hydrothermal carbonization temperature, Carbon 62 (2013) 346-355.
[26] M. Sevilla, A. Fuertes, R. Mokaya, High density hydrogen storage in superactivated carbons from hydrothermally carbonized renewable organic materials, Energy & Environmental Science 4(4) (2011) 1400-1410.
[27] C. Falco, J.M. Sieben, N. Brun, M. Sevilla, T. Van der Mauelen, E. Morallón, D. Cazorla-Amorós, M.M. Titirici, Hydrothermal Carbons from Hemicellulose-Derived Aqueous Hydrolysis Products as Electrode Materials for Supercapacitors, ChemSusChem 6(2) (2013) 374-382.
[28] S.-Y. Yang, K.-H. Chang, Y.-L. Huang, Y.-F. Lee, H.-W. Tien, S.-M. Li, Y.-H. Lee, C.-H. Liu, C.-C.M. Ma, C.-C. Hu, A powerful approach to fabricate nitrogen-doped graphene sheets with high specific surface area, Electrochemistry Communications 14(1) (2012) 39-42.
[29] M.A. Islam, M. Ahmed, W. Khanday, M. Asif, B. Hameed, Mesoporous activated carbon prepared from NaOH activation of rattan (Lacosperma secundiflorum) hydrochar for methylene blue removal, Ecotoxicology and environmental safety 138 (2017) 279-285.
[30] H. Wang, Z. Xu, A. Kohandehghan, Z. Li, K. Cui, X. Tan, T. Stephenson, C.K. King'ondu, C.M.B. Holt, B.C. Olsen, J.K. Tak, D. Harfield, P. Ajayan, D. Mitlin, Interconnected Carbon Nanosheets Derived from Hemp for Ultrafast Supercapacitors with High Energy, ACS Nano 7(6) (2013) 5131-5141.
[31] K. Foo, B. Hameed, Preparation and characterization of activated carbon from pistachio nut shells via microwave-induced chemical activation, Biomass and Bioenergy 35(7) (2011) 3257-3261.
[32] K. Foo, B. Hameed, Utilization of rice husks as a feedstock for preparation of activated carbon by microwave induced KOH and K2CO3 activation, Bioresour. Technol. 102(20) (2011) 9814-9817.
[33] Y. Lu, S. Zhang, J. Yin, C. Bai, J. Zhang, Y. Li, Y. Yang, Z. Ge, M. Zhang, L. Wei, Mesoporous activated carbon materials with ultrahigh mesopore volume and effective specific surface area for high performance supercapacitors, Carbon 124 (2017) 64-71.
[34] D. Zhao, J. Feng, Q. Huo, N. Melosh, G.H. Fredrickson, B.F. Chmelka, G.D. Stucky, Triblock copolymer syntheses of mesoporous silica with periodic 50 to 300 angstrom pores, science 279(5350) (1998) 548-552.
[35] L. Zou, L. Li, H. Song, G. Morris, Using mesoporous carbon electrodes for brackish water desalination, Water research 42(8) (2008) 2340-2348.
[36] S. Suganuma, K. Nakajima, M. Kitano, D. Yamaguchi, H. Kato, S. Hayashi, M. Hara, Hydrolysis of cellulose by amorphous carbon bearing SO3H, COOH, and OH groups, Journal of the American Chemical Society 130(38) (2008) 12787-12793.
[37] J. Barkauskas, M. Dervinyte, Investigation of the functional groups on the surface of activated carbons, Journal of the Serbian Chemical Society 69(5) (2004) 363-375.

[38] A. Reina, X. Jia, J. Ho, D. Nezich, H. Son, V. Bulovic, M.S. Dresselhaus, J. Kong, Large area, few-layer graphene films on arbitrary substrates by chemical vapor deposition, Nano letters 9(1) (2008) 30-35.
[39] Y. Liu, Y. Zhao, K. Li, Z. Wang, P. Tian, D. Liu, T. Yang, J. Wang, Activated carbon derived from chitosan as air cathode catalyst for high performance in microbial fuel cells, Journal of Power Sources 378 (2018) 1-9.
[40] S. Xu, L. Yong, P. Wu, One-pot, green, rapid synthesis of flowerlike gold nanoparticles/reduced graphene oxide composite with regenerated silk fibroin as efficient oxygen reduction electrocatalysts, ACS applied materials & interfaces 5(3) (2013) 654-662.
[41] O. Maslova, M. Ammar, G. Guimbretière, J.-N. Rouzaud, P. Simon, Determination of crystallite size in polished graphitized carbon by Raman spectroscopy, Physical Review B 86(13) (2012) 134205.
[42] M. Matthews, M. Pimenta, G. Dresselhaus, M. Dresselhaus, M. Endo, Origin of dispersive effects of the Raman D band in carbon materials, Physical Review B 59(10) (1999) R6585.
[43] Z. Tai, Q. Zhang, Y. Liu, H. Liu, S. Dou, Activated carbon from the graphite with increased rate capability for the potassium ion battery, Carbon 123 (2017) 54-61.
[44] M. Keeping, O. Reynolds, Silicon in agriculture: new insights, new significance and growing application, Annals of Applied Biology 155(2) (2009) 153.
[45] D. Yang, A. Velamakanni, G. Bozoklu, S. Park, M. Stoller, R.D. Piner, S. Stankovich, I. Jung, D.A. Field, C.A. Ventrice, Chemical analysis of graphene oxide films after heat and chemical treatments by X-ray photoelectron and Micro-Raman spectroscopy, Carbon 47(1) (2009) 145-152.
[46] M. Seah, The quantitative analysis of surfaces by XPS: a review, Surface and Interface Analysis 2(6) (1980) 222-239.
[47] M. Smíšek, S. Černý, Active carbon: manufacture, properties and applications, Elsevier Publishing Company1970.
[48] M. Lillo-Ródenas, D. Cazorla-Amorós, A. Linares-Solano, Understanding chemical reactions between carbons and NaOH and KOH: an insight into the chemical activation mechanism, Carbon 41(2) (2003) 267-275.
[49] M. Lillo-Ródenas, J. Juan-Juan, D. Cazorla-Amorós, A. Linares-Solano, About reactions occurring during chemical activation with hydroxides, Carbon 42(7) (2004) 1371-1375.
[50] L.M. Viculis, J.J. Mack, R.B. Kaner, A chemical route to carbon nanoscrolls, Science 299(5611) (2003) 1361-1361.